Experimental investigation of polarization modulation instability in a double-clad single-mode tellurite optical fiber

Tonglei Cheng[1] · Fan Zhang[1] · Shuguang Li[1] · Xin Yan[1] · Fang Wang[1] · Xuenan Zhang[1] · Takenobu Suzuki[2] · Yasutake Ohishi[2]

Abstract

A double-clad single-mode tellurite optical fiber (DC-SMTOF) with a loss of 0.5 dB/m @1545.1 nm was fabricated based on the TeO_2–ZnO–Li_2O–Bi_2O_3 (TZLB) material. During the fiber drawing process, a low level of residual birefringence was produced, which gave a chance for the investigation of the polarization modulation instability (PMI). With a nanosecond laser operated at 1545.1 nm as the pump source, the PMI effect in the DC-SMTOF was investigated using different fiber length and different average pump power. This investigation of the PMI generation in non-silica optical fibers may provide guidance for the generation of the highly repetitive optical pulse train.

1 Introduction

Modulation instability (MI) is a nonlinear four-wave mixing process in which the amplitude and phase modulations of a wave grow as a result of an interplay between the nonlinear and dispersive effects, and the energy is exchanged between an intense pump wave and two weak sideband waves [1–4]. When MI was first observed in optical fibers [1], it was regarded possible only in the anomalous dispersion regime, because the nonlinear phase mismatch of this regime is positive, while MI requires a negative one to occur [5–7]. Therefore, extensive investigations have been carried out concerning MI in the anomalous dispersion regime of various optical fibers [8, 9]. However, in the birefringence optical fibers, MI process may occur in the normal dispersion regime, among which is the polarization modulation instability (PMI) [10–13], where the coupling induced by the two orthogonally polarized wave contributes to the linear phase mismatch and, therefore, plays a predominant role in the phase-matching condition [5].

PMI was first theoretically predicted in 1970 by Berkhoer et al. [14], and since then, many investigations concerning PMI have been conducted. In 1988, Wabnitz et al. reported PMI in a nonlinear birefringent dispersive medium [15]. In 1995 Murdoch et al. published the first experimental observation of PMI in a weakly birefringent optical fibers [16]. Kruhlak et al. investigated PMI effect in a photonic crystal fiber (PCF) in 2006 [17]. Frisquet et al. demonstrated the generation of PMI sidebands in the normal dispersion regime of a relatively long span of dispersion-compensating fiber in 2015 [18]. Recently, Fatome et al. reported the observation of PMI process occurring in a fiber Kerr resonator [19]. Zhang et al. reported isotropic PMI in single-mode conventional telecom fibers [20]. Despite the extensive exploration in nonlinear media or silica optical fibers, PMI in soft-glass optical fibers with high nonlinear refractive index has not been touched yet.

Tellurite optical fibers have high nonlinear refractive indices and wide transmission window in the mid-infrared region [21–24], which have already been applied to fiber sensors, fiber lasers and amplifiers, etc. [25–27]. They provide a desirable platform for PMI generation.

In this paper, a double-clad single-mode tellurite optical fiber (DC-SMTOF) was fabricated based on the TeO_2–ZnO–Li_2O–Bi_2O_3 (TZLB) material. With a nanosecond laser operated at ~ 1545.1 nm as the pump source, PMI was experimentally demonstrated. Furthermore, the influence of fiber length and average pump power on the PMI effect was investigated.

✉ Xuenan Zhang
    zhangxuenan@ise.neu.edu.cn

[1] State Key Laboratory of Synthetical Automation for Process Industries, College of Information Science and Engineering, Northeastern University, Shenyang 110819, China

[2] Research Center for Advanced Photon Technology, Toyota Technological Institute, Nagoya 468-8511, Japan

2 Fabrication and property of the DC-SMTOF

The DC-SMTOF was fabricated following the three-step process using the rod-in-tube drawing technique, as detailed previously [28]. During the fiber drawing process, a very low level of the residual birefringence was produced, which gave a chance for the generation of PMI in the DC-SMTOF [20]. Compared to the single cladding optical fibers, the double cladding structure can improve the light confinement ability and reduce the fiber loss.

Figure 1 shows the group velocity dispersion (GVD) of the fundamental mode in the DC-SMTOF, which was calculated using the full-vectorial mode solver (MODE SOLUTIONS). The SEM image of fiber's cross-section is presented in the inset, and the diameter was ~ 2.45 μm. The diameter of the 1st and 2nd cladding was ~ 33 and 124 μm, respectively. The linear refractive index of the core material was 2.05, and the refractive index difference between the core and the first cladding was ~ 2.0%@ ~ 1545.1 nm, which
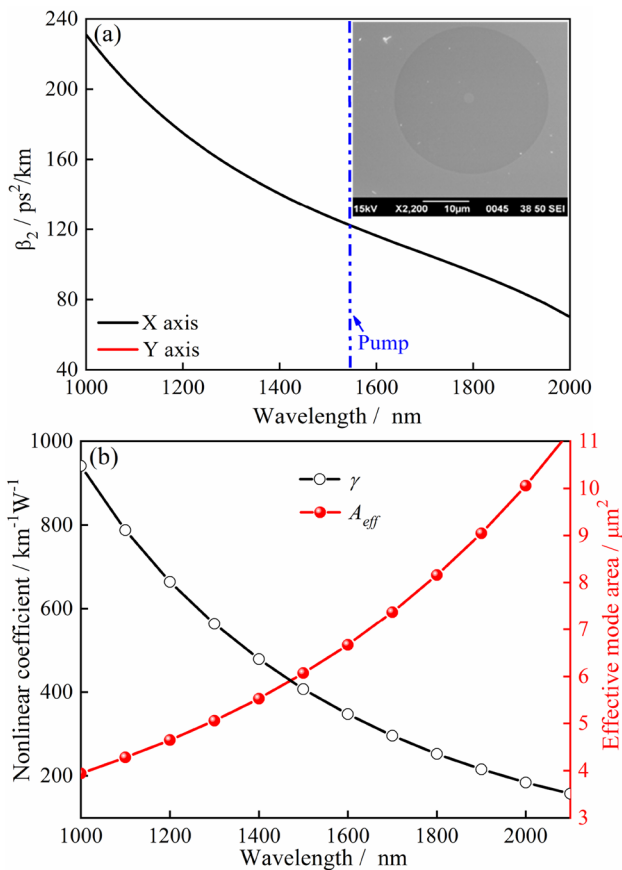
Fig. 1 a Calculated GVDs of the fundamental mode. Inset is cross-section of the DC-SMTOF. **b** Calculated nonlinear coefficient and effective mode area

were measured using prisms based on the glass samples. The measured values were fitted to the Sellmeier formula to obtain Sellmeier coefficients shown in Table 1. The attenuation of the tellurite fiber was ~ 0.5 dB/m @ ~ 1545.1 nm, measured by the cutback technique. The nonlinear coefficient and the effective mode area were calculated, as shown in Fig. 1b.

3 Experiment results and discussion

The experimental setup is shown in Fig. 2. The pump source was a nanosecond laser with a pulse width of ~ 4.1 ns and a repetition rate of ~ 25 kHz. The center wavelength of the pump source was ~ 1545.1 nm, which located within the normal dispersion regime of the DC-SMTOF. A polarization controller (PC) was used in the experiment to control the polarization state. A fiber collimator (FC) helped to form a free-space collimated beam which, after passing through a neutral density (ND) filter and a half-wave plate (HWP), was coupled into the DC-SMTOF fiber core by an aspheric lens (AL) with a focal length of ~ 6.24 mm and an numerical aperture (NA) of ~ 0.40 (NEWPORT, F-LA11, 510–1550 nm). Finally, an optical spectrum analyzer (OSA, Yokogawa) using a single mode fiber (SMF)

Table 1 Sellmeier coefficients of the core and the first cladding glasses

$n^2(\lambda) = 1 + \sum_{i=1}^{3} \frac{A_i \lambda^2}{\lambda^2 - L_i^2}$

	Core glass		First cladding glass	
	A_i	L_i/μm	A_i	L_i/μm
1	1.67189	0.0216	1.63758	0.02193
2	1.34862	0.23971	1.34201	0.24061
3	0.62186	6.8356	0.65885	6.97016
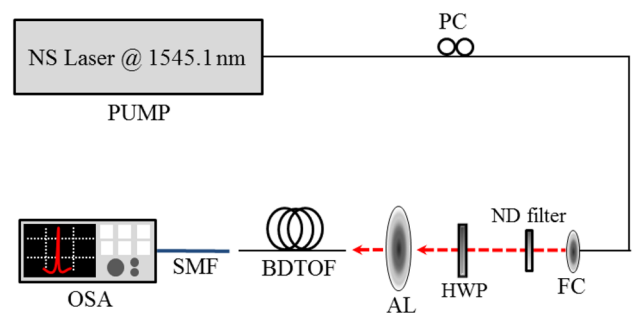
Fig. 2 Experimental setup for investigating MI in the DC-SMTOF. *PC* polarization controller, *FC* fiber collimator, *HWP* half-wave plate, *AL* aspheric lens, *SMF* single mode fiber, *OSA* optical spectrum analyzer

was used to record the output spectrum from the other end of the DC-SMTOF.

We first fed the experimental system with a 2.5 m DC-SMTOF and an average pump power of 47 mW. With the rotation of the HWP, the observed MI effect evolved regularly. The azimuth of the HWP was regarded as 0° at the occurrence of the maximal MI, as shown in Fig. 3a. When the HWP shifted to 45°, the sidebands disappeared and no MI effect was observed, as shown in Fig. 3b. After that, with the every shift of 45°, the MI spectrum would gradually change from none to the maximal and the maximal to none. From this experimental observation, we can conclude that the generated MI process was closely associated with the polarization state. Then an analyzer was connected to the output end of the DC-SMTOF, and we found that both of the sidebands were orthogonal to the polarization state of the pump. The above observation was consistent with the properties of PMI stated in [5, 20], so we confirmed that the MI generated in this DC-SMTOF was PMI. To the best of our knowledge, it was the first demonstration of PMI in the
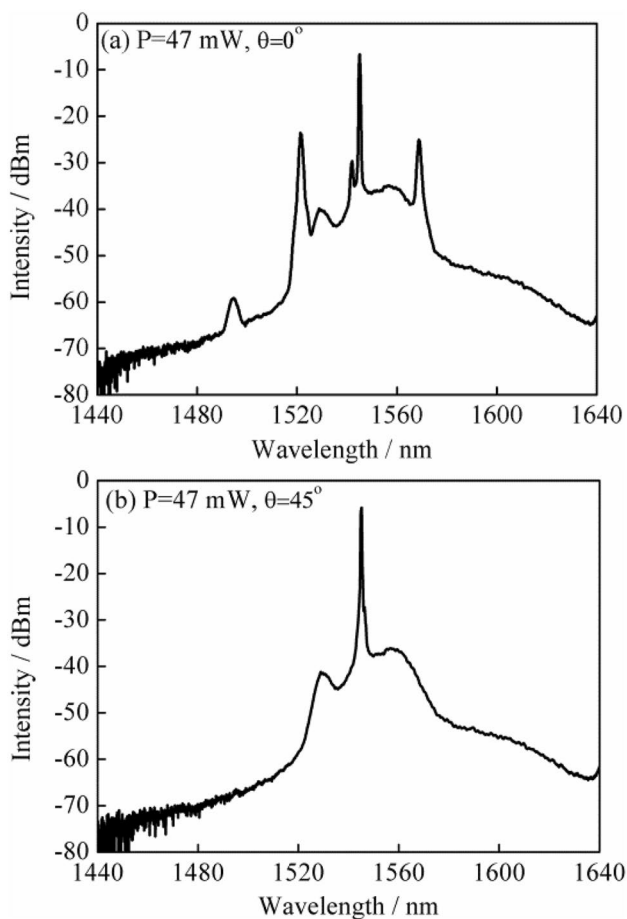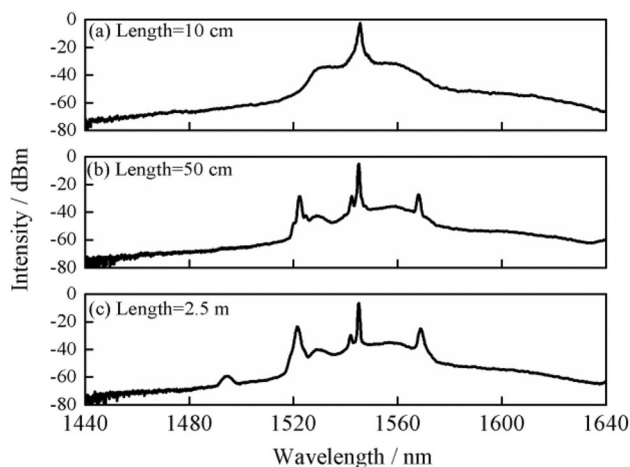
tellurite optical fibers, which may provide guidance to the generation of the highly repetitive optical pulse train.

To investigate the effect of fiber length on PMI effect, the DC-SMTOFs of 10, 50 and 2.5 m were tried out in turns at the average pump power of 47 mW. The output spectra are shown in Fig. 4, where the intensity of the output peak power dwindled continually (0.58, 0.31 and 0.22 mW, respectively), while the PMI effect became more and more obvious. This was because the fiber length has a direct influence on the fiber loss as well as the intensity of the nonlinear effect. The longer the length, the larger the loss and in turn the more damage to the output peak power. On the other hand, The longer the length, the stronger the nonlinear effect, and the more obvious the PMI. During the following investigation, the 2.5 m DC-SMTOF was used to guarantee the easy observation of the PMI spectrum.

To investigate the influence of average pump power on the PMI effect, the average pump power was adjusted within the range of 6.5–126 mW, and the measured PIM spectra are shown in Fig. 5. At 6.5 mW, no PMI was observed due to the low pump power, and the spectrum can be considered as that from the laser source. When the average pump power increased to 15 mW, the first order (1st) PMI was observed. At 19 mW, the second order (2nd) PMI was obtained, but due to the noise from the laser and the SRS, the Stokes band was not obvious. When the average pump power increased to 26.5 mW, the third order (3rd) PMI appeared, together with a more prominent 2nd Stokes band. However, with the further increase of the average pump, at 47 mW the 3rd PMI disappeared, and from 70 to 126 mW only the 1st PMI survived. From the figure we can see that the PMI effect became more and more prominent till 26.5 mW and then began to turn weak. The 1st PMI persisted throughout the whole experiment process, but it was also subject to the

Fig. 3 **a** MI in the 2.5 m DC-SMTOF at the azimuth of 0°. **b** MI in the 2.5 m DC-SMTOF at the azimuth of 45°

Fig. 4 Experimental output spectra of the DC-SMTOF at the average pump power of 47 mW with different fiber lengths. **a** 10 cm; **b** 50 cm; **c** 2.5 m
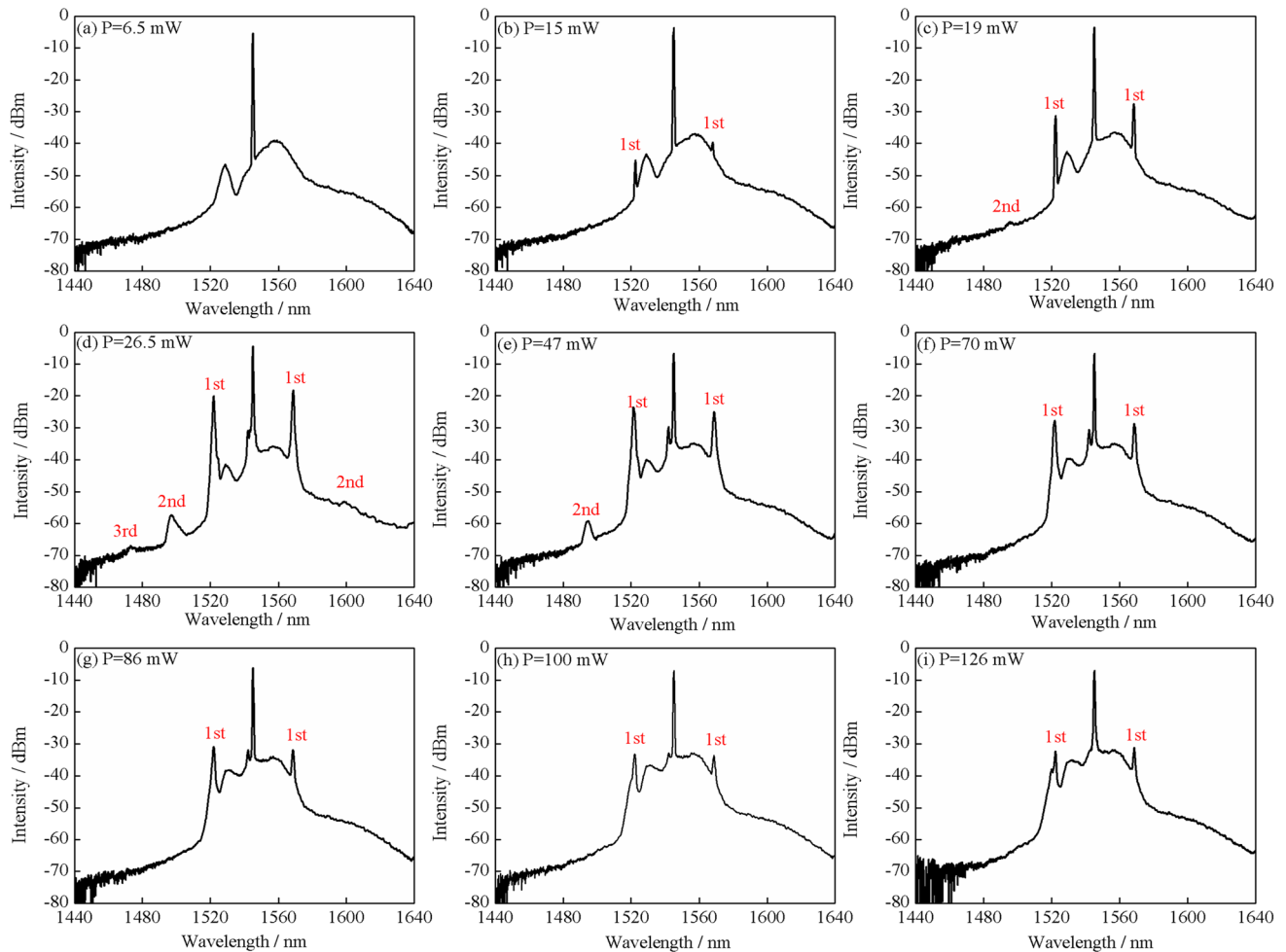
Fig. 5 PMI spectra at the average pump power of 6.5, 15, 19, 26.5, 47, 70, 86, 100 and 126 mW

variation of the average pump power, which can be clearly seen from the following investigation.

Figure 6a shows the evolution of the 1st PMI's total average output power (P_{total}) and peak power (P_{peak}) at the average pump power range of 6.5 ~ 126 mW, both of which were measured by OSA from 1440 to 1640 nm. Figure 6b shows the peak power of the 1st PMI sidebands (P_{Stokes} and $P_{Anti-Stokes}$). From 6.5 to 26.5 mW, P_{total} and P_{peak} increased continuously, together with P_{Stokes} and $P_{Anti-Stokes}$. At 26.5 mW, we obtained the maximal $P_{total} = 574.9$ μW, $P_{peak} = 485$ μW, $P_{Stokes} = 15.03$ μW and $P_{Anti-Stokes} = 9.91$ μW. After the average pump power exceeded 26.5 mW, P_{total}, P_{peak}, P_{Stokes} and $P_{Anti-Stokes}$ plunged sharply. Figure 6c shows the wavelengths of the 1st PMI's Stokes and anti-Stokes bands. From 15 to 26.5 mW, both of the two wavelengths shifted far away from the pump wavelength, which indicated the PMI effect became continuously stronger. At 26.5 mW, the maximal wavelength shift was obtained, being 1568.8 and 1521.7 nm respectively. With the further increase of the average pump power, both wavelengths began to draw
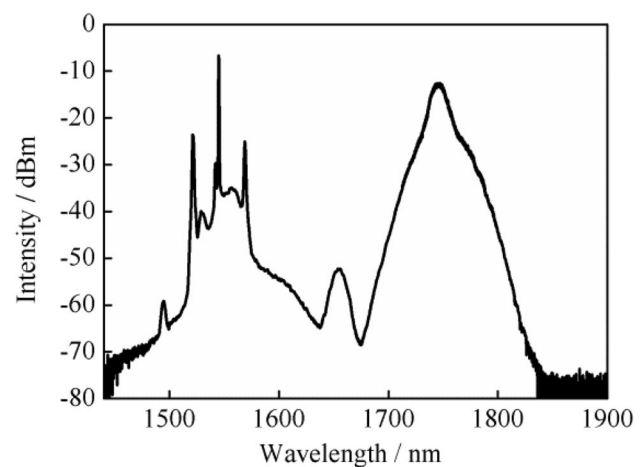
nearer to the central pump wavelength, for the PMI effect was weakening with the increase of the average pump power. From these three figures we can see clearly that the 1st PMI was also under the influence of the average pump power variation.

The above experimental observation showed that the PMI effect did not simply go stronger with the increase of the average pump power, which was different from its regular evolution pattern. To reveal the reason behind it, the experimental spectrum from 1440 to 1900 nm was recorded at the average pump power of 47 mW, as shown in Fig. 7. Because the pump wavelength (~ 1545.1 nm) located within the normal dispersion regime of the DC-SMTOF, the stimulated Raman scattering (SRS) could occur easily. From the figure we can see that at 1745 nm strong SRS was observed, for the pump power satisfied the threshold of Raman scattering. From 1440 to 1900 nm, the total output average power at the end of the DC-SMTOF was measured to be 2.462 mW by OSA. However, from 1600 to 1900 nm, the power of SRS was 2.121 mW (accounting for 86.1% of the total power), which indicated that
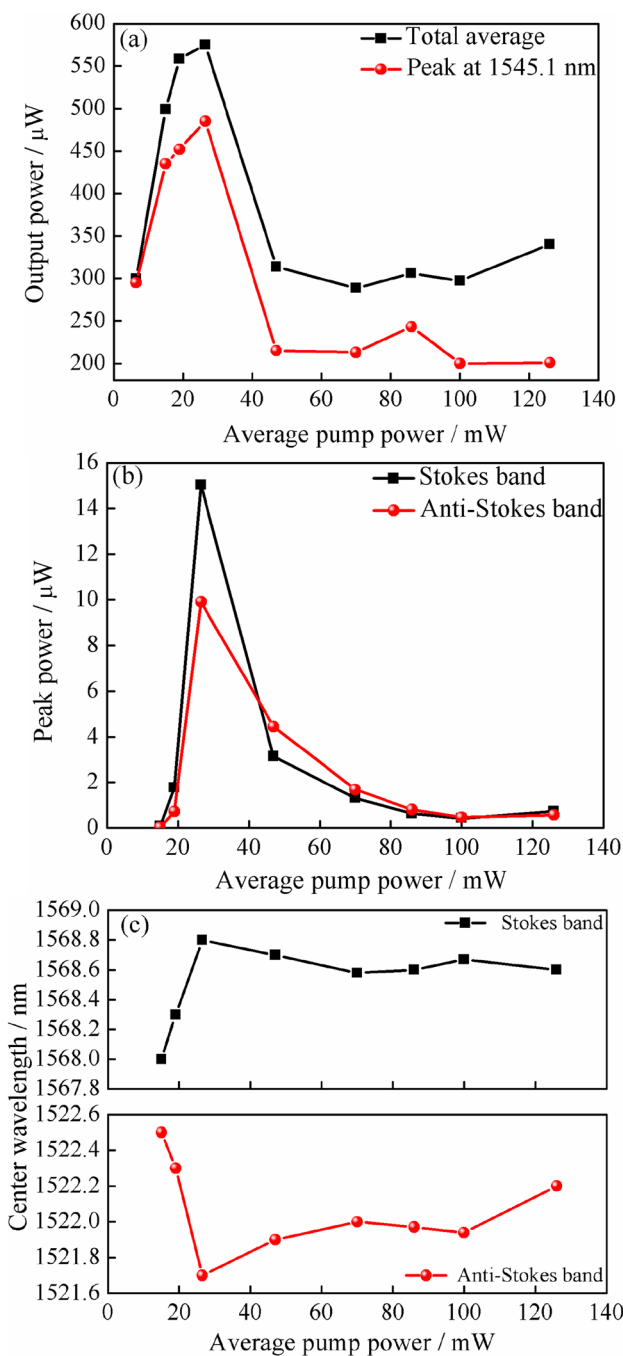
Fig. 6 **a** Total average output power and peak output power of the 1st PMI at different average pump power. **b** Peak power of Stokes and anti-Stokes bands of the 1st PMI at different average pump power. **c** Wavelengths of Stokes and anti-Stokes bands of the 1st PMI at different average pump power

Fig. 7 Experimentally measured spectrum from the end of the DC-SMTOF at the wavelength region of 1440–1900 nm with the output average power of 2.462 mW

pattern, where the PMI effect first went strong and then turned weak with the increase of the average pump power.

4 Conclusions

We experimentally demonstrated the PMI generation and evolution in a DC-SMTOF. First the relationship between the polarization state and the MI effect was investigated, which helped confirm the generation of PMI. Then the effect of fiber length on PMI effect was investigated, which showed that the longer the fiber, the stronger the PMI effect. Next the influence of the average pump power variation was investigated, where the PMI effect became more and more prominent till 26.5 mW and then began to turn weak. This was because after 26.5 mW, SBS became increasingly prominent, which carried power away from the pump and severely affected the generation of PMI. This investigation of the PMI generation in the DC-SMTOF with the weak level of residual birefringence may provide the potential application in generating the optical pulse train with a high repetition rate.

References

1. K. Tai, A. Hasegawa, A. Tomita, Observation of modulational instability in optical fibers. Phys. Rev. Lett. **56**, 135–138 (1986)

SRS carried most of the power away from the pump and made the pump depletion. After the average pump power exceeded 26.5 mW, the SRS effect became increasingly prominent and carried more power away from the pump, which severely affected the generation of PMI. This resulted in the evolution

2. G.P. Agrawal, *Nonlinear Fiber Optics*, 5th edn. (Academic, San Francisco, 2013)

3. R.H. Stolen, Phase-matched-stimulated four-photon mixing in silica-fiber waveguides. IEEE J. Quantum Electron. **11**, 100–103 (1975)

4. G. Millot, S. Pitois, P. Tchofo Dinda, M. Haelterman, Observation of modulational instability induced by velocity-matched cross-phase modulation in a normally dispersive bimodal fiber. Opt. Lett. **22**, 1686–1688 (1997)

5. A. Kudlinski, A. Bendahmane, D. Labat, S. Virally, R.T. Murray, E.J.R. Kelleher, A. Mussot, Simultaneous scalar and cross-phase modulation instabilities in highly birefringent photonic crystal fiber. Opt. Express **21**, 8437–8440 (2013)

6. P. Kockaert, M. Haelterman, S. Pitois, G. Millot, Isotropic polarization modulational instability and domain walls in spun fibers. Appl. Phys. Lett. **75**, 2873–2875 (1999)

7. P. Tchofo Dinda, K. Porsezian, Impact of fourth-order dispersion in the modulational instability spectra of wave propagation in glass fibers with saturable nonlinearity. J. Opt. Soc. Am. B **27**, 1143–1152 (2010)

8. J. Zhang, Q. Li, W. Pan, S.Y. Luo, Y.L. Chen, Self-induced phase matching in stimulated four-wave mixing in a nonbirefringent single-mode optical fiber. Opt. Lett. **26**, 214–216 (2001)

9. A. Armaroli, S. Trillo, Modulational instability due to cross-phase modulation versus multiple four-wave mixing: the normal dispersion regime. J. Opt. Soc. Am. B **31**, 551–558 (2014)

10. P.D. Drummond, T.A.B. Kennedy, J.M. Dudley, R. Leonhardt, J.D. Harvey, Cross-phase modulational instability in high-birefringence fibers. Opt. Commun. **78**, 137–142 (1990)

11. J.S.Y. Chen, G.K.L. Wong, S.G. Murdoch, R.J. Kruhlak, R. Leonhardt, J.D. Harvey, N.Y. Joly, J.C. Knight, Cross-phase modulation instability in photonic crystal fibers. Opt. Lett. **31**, 873–875 (2006)

12. E.E. Serebryannikov, S.O. Konorov, A.A. Ivanov, M.V. Alfimov, M. Scalora, A.M. Zheltikov, Cross-phase-modulation-induced instability in photonic-crystal fibers. Phys. Rev. E **72**, 027601 (2005)

13. T. Godin, Y. Combes, R. Ahmad, M. Rochette, T. Sylvestre, J.M. Dudley, Far-detuned mid-infrared frequency conversion via normal dispersion modulation instability in chalcogenide microwires. Opt. Lett. **39**, 1885–1888 (2014)

14. A.L. Berkhoer, V.E. Zakharov, Self excitation of waves with different polarizations in nonlinear media. Sov. Phys. JETP **31**, 486–490 (1970)

15. S. Wabnitz, Modulational polarization instability of light in a nonlinear birefringent dispersive medium. Phys. Rev. A **38**, 2018–2021 (1988)

16. S.G. Murdoch, R. Leonhardt, J.D. Harvey, Polarization modulation instability in weakly birefringent fibers. Opt. Lett. **20**, 866–868 (1995)

17. R.J. Kruhlak, G.K.L. Wong, J.S.Y. Chen, S.G. Murdoch, R. Leonhardt, J.D. Harvey, N.Y. Joly, J.C. Knight, Polarization modulation instability in photonic crystal fibers. Opt. Lett. **31**, 1379–1381 (2006)

18. B. Frisquet, B. Kibler, J. Fatome, P. Morin, F. Baronio, M. Conforti, G. Millot, S. Wabnitz, Polarization modulation instability in a Manakov fiber system. Phys. Rev. A **92**, 053854 (2015)

19. J. Fatome, B. Kibler, F. Leo, A. Bendahmane, G.-L. Oppo, B. Garbin, Y. Wang, S.G. Murdoch, M. Erkintalo, S. Coen, Polarization modulation instability in a fiber Kerr resonator. Nonlinear Photonics (Zurich Switzerland) **2018**, NpTu4C.6 (2018)

20. H. Zhang, M. Gilles, M. Guasoni, B. Kibler, A. Picozzi, J. Fatome, Isotropic polarization modulational instability in single-mode conventional telecom fibers. JOSA B **36**(9), 2445–2451 (2019)

21. T.H. Tuan, S. Kuroyanagi, K.O. Nagasaka, T. Suzuki, Y. Ohishi, Near-infrared optical image transport through an all-solid tellurite optical glass rod with transversely-disordered refractive index profile. Opt. Express **26**, 16054–16062 (2018)

22. T.L. Cheng, L. Zhang, X. Xue, D. Deng, T. Suzuki, Y. Ohishi, Broadband cascaded four-wave mixing and supercontinuum generation in a tellurite microstructured optical fiber pumped at 2 μm. Opt. Express **23**, 4125–4134 (2015)

23. J. Picot-Clemente, C. Strutynski, F. Amrani, F. Désévédavy, J.C. Jules, G. Gadret, D. Deng, T.L. Cheng, K. Nagasaka, Y. Ohishi, B. Kibler, F. Smektala, Enhanced supercontinuum generation in tapered tellurite suspended core fiber. Opt. Express **23**, 4125–4134 (2015)

24. M. Belal, L. Xu, P. Horak, L. Shen, X. Feng, M. Ettabib, D.J. Richardson, P. Petropoulos, J.H.V. Price, Mid-infrared supercontinuum generation in suspended core tellurite microstructured optical fibers. Opt. Lett. **40**, 2237–2240 (2015)

25. X. Wu, P. Huang, T.Y. Huang, Z.C. Wu, Z. Cheng, B.W. Chen, K.X. Ren, S.N.A. Fu, Tunable all-optical actively mode-locked fiber laser at 2 μm based on tellurite photonic crystal fiber. Laser Phys. Lett. **15**, 065103 (2018)

26. T. Cheng, S. Tanaka, T.H. Tuan, T. Suzuki, Y. Ohishi, All-optical dynamic photonic bandgap control in an all-solid double-clad tellurite photonic bandgap fiber. Opt. Lett. **42**, 2354–2357 (2017)

27. A. Mori, Tellurite-based fibers and their applications to optical communication networks. J. Ceram. Soc. Jpn. **116**, 1040–1051 (2008)

28. T. Cheng, Y. Xiao, S. Li, X. Yan, X. Zhang, T. Suzuki, Y. Ohishi, Highly efficient second-harmonic generation in a tellurite optical fiber. Opt. Lett. **44**, 4686–4689 (2019)